European Journal of Radiology 116 (2019) 90–97

Contents lists available at ScienceDirect

European Journal of Radiology

journal homepage: www.elsevier.com/locate/ejrad

Research article

Diagnostic performance of fractional flow reserve derived from coronary CT angiography for detection of lesion-specific ischemia: A multi-center study and meta-analysis

Chun Xiang Tang[a,1], Yi Ning Wang[b,1], Fan Zhou[a], U. Joseph Schoepf[a,c], Marly van Assen[c], Robert E. Stroud[c], Jian Hua Li[d], Xiao Lei Zhang[a], Meng Jie Lu[a], Chang Sheng Zhou[a], Dai Min Zhang[e], Yan Yi[b], Jing Yan[f], Guang Ming Lu[a], Lei Xu[g,*], Long Jiang Zhang[a,*]

[a] Department of Medical Imaging, Jinling Hospital, Medical School of Nanjing University, Nanjing, Jiangsu 210002, China
[b] Department of Radiology, Peking Union Medical College Hospital, Chinese Academy of Medical Sciences and Peking Union Medical College, Beijing, 100730, China
[c] Division of Cardiovascular Imaging, Department of Radiology and Radiological Science, Medical University of South Carolina, Ashley River Tower, MSC 226, 25 Courtenay Dr, Charleston, SC 29425, United States
[d] Department of Cardiology, Jinling Hospital, Medical School of Nanjing University, Nanjing, Jiangsu 210002, China
[e] Department of Cardiology, Nanjing First Hospital, Nanjing Medical University, Nanjing, Jiangsu 210006, China
[f] Siemens Healthcare Ltd., No. 278 ZhouZhu Road, Shanghai 201318, China
[g] Department of Radiology, Beijing Anzhen Hospital, Capital Medical University, Beijing 10029, China

ARTICLE INFO

Keywords:
Fractional flow reserve
Coronary CT angiography
Coronary artery disease
Computational fluid dynamics
Machine learning
Multicenter study
Meta analysis

ABSTRACT

Purpose: To evaluate the diagnostic performance of coronary computed tomography angiography derived fractional flow reserve (CT-FFR) with invasive fractional flow reserve (FFR) in patients with coronary artery disease" before "with invasive fractional flow reserve serving as the reference standard.

Materials and methods: CT-FFR values based on a machine learning algorithm ($cFFR_{ML}$) in 183 vessels of 136 patients from four centers were measured with invasive FFR as reference standard. The diagnostic performance from our multicenter study was combined into a meta-analysis following a literature search in Web of Science, PubMed, Cochrane library to identify studies comparing diagnostic performance of coronary computed tomography angiography (CCTA) and CT-FFR. Sensitivity, specificity, accuracy were analyzed on both per-vessel and per-patient basis for intermediate lesions and by algorithm.

Results: Our multicenter study demonstrated sensitivities, specificities, and accuracies of $cFFR_{ML}$ and CCTA of 0.85, 0.94, 0.90, and 0.95, 0.28, 0.55 on a per-vessel basis, respectively. For our meta-analysis, pooled sensitivities, specificities, and accuracies of CT-FFR and CCTA were 0.85, 0.82, 0.82, and 0.85, 0.57, 0.65 with AUC of 0.86 (95%CI: 0.83˜0.89) and 0.83 (95%CI: 0.79˜0.86) on a per-vessel basis, respectively. The sensitivity, specificity and accuracy for intermediate lesions using $cFFR_{ML}$ were 0.84, 0.92, and 0.89. No significant difference was found among different algorithms of CT-FFR ($P < 0.001$).

Conslusion: This multicenter study with meta-analysis showed that CT-FFR had a high diagnostic accuracy in determining ischemia-specific lesions and intermediate lesions. There was no significant difference when comparing the combined diagnostic performance of different algorithms of CT-FFR with invasive FFR as the reference standard.

Abbreviations: CAD, coronary artery disease; CFD, computational fluid dynamics; CCTA, coronary computed tomography angiography; $cFFR_{ML}$, computational CT-FFR based on machine learning algorithm; CI, confidence interval; DOR, diagnostic odds ratio; FFR, fractional flow reserve; CT-FFR, fcoronary CT angiography derived fractional flow reserve; FFR_{CT}, fractional flow reserve derived from coronary computed tomography angiograph form HeartFlow Inc., Redwood City, California; LR+, positive likelihood ratio; LR−, negative likelihood ratio; NPV, negative predictive value; PPV, positive predictive value; QUADAS-2, Quality Assessment of Diagnostic Accuracy Studies, Version 2; SROC curve, summary receiver operating characteristic curve

* Corresponding authors.
E-mail addresses: leixu2001@hotmail.com (L. Xu), kevinzhlj@163.com, kevinzhlj@nju.edu.cn (L.J. Zhang).
[1] These authors made the same contribution to this study.

https://doi.org/10.1016/j.ejrad.2019.04.011
Received 12 December 2018; Received in revised form 3 April 2019; Accepted 19 April 2019

1. Introduction

Coronary computed tomography angiography (CCTA) is an established non-invasive modality for evaluation of coronary artery disease (CAD); however, this technique is unable to determine the hemodynamic relevance of coronary stenosis [1]. The quantification of functional coronary stenosis is vital for patient management to prevent mortality from CAD. Though fractional flow reserve (FFR) is the gold standard for determining the functional severity of lesions, the use of FFR is relatively uncommon due to additional costs, the need to administrate drugs to induce hyperemia, and the invasive nature of the measurement [2].

Noninvasive CCTA derived FFR (CT-FFR) has been expolited to determine myocardial ischemia, guide therapeutic strategies and provide prognostic assessment. By applying the principles of computational fluid dynamics (CFD) and image-based modelling from CCTA images, this technique permits computation of coronary flow and pressures along the length of the entire coronary tree. The first and most recognized FFR derived from CCTA (FFR_{CT}) was validated the value of this modality with three multicenter clinical trials [4–6] with improved diagnostic accuracy in differentiating ischemic and non-ischemic stenosis compared with CCTA alone with invasive FFR as the reference standard. However, FFR_{CT} requires the use of off-site supercomputers, which can be time consuming and markedly limit the clinical utility of CT-FFR [1]. Thus, the development of a instantly available CT-FFR technique for the clinical setting is warranted. This essential requirement stimulates innovative solutions from different vendors for physician-driven CT-FFR using regular on-site workstation with CFD algorithm to identify myocardial ischemia in patients with CAD [6–11]. More recently, an additional approach has emerged based on deep machine learning methods by using an artificial intelligence algorithm to compute the functional severity of lesions [12–14]. Compared with the physics-based CFD model, the average computation time of machine learning-based CT-FFR was reduced more than 80-fold, allowing near real-time assessment of CT-FFR [6]. Although the diagnostic performance of machine learning-based CT-FFR has been previously investigated with comparable accuracy to CFD-based CT-FFR [7,15,16], the clinical implementation and in-hospital availability of this new technique still remain problematic. Moreover, the combined diagnostic performance of different algorithms of noninvasive FFR derived from CCTA remains unclear.

Previous meta-analyses have evaluated the diagnostic performance of FFR_{CT} both at the per-patient level and the per-vessel or per-lesion level as defined by invasive FFR [17,18], assessed the combined diagnostic performance with off-site FFR_{CT} and on-site CFD-based CT-FFR [19–21]. However, concerns have been raised about the applicability of univariate model in pooling estimates of sensitivity and specificity, either with fixed- or random-effects model, which might inadvertently produce inaccurate results by ignoring threshold effects and correlation between the two estimates [22]. Moreover, results of other on-site CFD-based CT-FFR and new machine learning-based CT-FFR have recently been published [1,6]. Therefore, an updated meta-analysis was needed to comprehensively search and review evidence available heretofore and derive reliable assessment of the diagnostic performances of CT-FFR as the method for pooling diagnostic measures.

Thus, the purpose of this study was twofold: (a) to evaluate the diagnostic accuracy of a new noninvasive CT-FFR algorithm that is based on the deep machine learning method with a large sample size from multiple centers and (b) to review the combined diagnostic performance of different algorithms of CT-FFR and CCTA with invasive FFR serving as the reference standard to estimate lesion specific ischemia from a collection of currently existing reports on CT-FFR studies in patients with suspected or known CAD.

2. Methods

2.1. Study protocol

This retrospective multi-center study was performed from May 1, 2015 to December 31, 2017 at four medical centers in China. The written informed patient consent and research ethic approval were obtained for this study. A total of 147 patients were included. All patients underwent CCTA for the evaluation of suspected or known CAD and were subsequently referred to invasive coronary angiography within 60 days of CCTA. Invasive FFR was measured for at least one coronary lesion. The flowchart of this multicenter study is displayed in Supplementary Fig. 1.

2.2. Coronary CT angiography image acquisition protocol

CCTA was performed using CT scanners with ≥64 detector rows (Somatom Flash/Force; Siemens Medical Solutions, Germany). Sublingual nitroglycerin (0.1 mg per dose, Nitroglycerin Inhaler; Jingwei Pharmacy Co, Ltd, Jinan, China) was given 5 min prior to scanning the patients. Beta-blockers were not administered to any of the patients. All 136 patients underwent CCTA with prospectively ECG-triggered adaptive sequence acquisition. Acquisition parameters were as follows: detector collimation, 64 × 2 × 0.6 mm/96 × 2 × 0.6 mm; gantry rotation time, 280 ms/250 ms ms; and effective tube current–time product, 370 mAs per rotation. For all studies, automated tube current modulation (CAREDose 4D, Siemens) and automated tube voltage modulation (CAREKV, Siemens) were enabled. Image acquisition was prospectively triggered to the patient's ECG at 30%–80% of the R-R interval per our routine clinical practice of CCTA with a section thickness of 0.75 mm, a reconstruction increment of 0.5 mm, and a medium soft-tissue convolution reconstruction kernel (I26f/ Bv40). Patients received 60 mL of iopromide (Ultravist 370 mg I/mL, Bayer Schering Pharma, Berlin, Germany) via injection into an antecubital vein using a 20-gauge catheter with a flow rate of 4˜5 mL/s. The bolus tracking technique was employed by placing a region of interest in the aortic root in order to detect bolus arrival. Image acquisition began 4 s after an attenuation threshold of 100 Hounsfield Units was achieved.

Only good or excellent CCTA image quality assessed using a four-point Likert scale [23] were included. Stenosis severity with luminal diameter reduction was visually assessed by two experienced local investigators (F.Z. and L.X.Z) in coronary vessel segments ≥2 mm in diameter according to CCTA. Stenosis severity > 50% was defined as lesion-specific ischemia on CCTA, and 30%–70% of stenosis severity were considered intermediate lesions according to previous studies [4–6].

2.3. CT-FFR Image analysis

All machine learning based CT-FFR calculations were performed on routine CCTA datasets using a software prototype (cFFR, version 3.0.0, Siemens). The software is based on an artificial intelligence deep machine learning ($cFFR_{ML}$) platform for the noninvasive computation of FFR values using CCTA data [12–15,24]. A reduced-order CFD model was used to compute the pressure and flow distribution for each coronary tree. Subsequently, quantitative features of the coronary anatomy and computed FFR values were extracted at each location along the coronary tree and the deep machine learning algorithm was trained to learn the relationship between the FFR values and quantitative anatomic features [1,6].

CCTA were reconstructed with a section thickness of 0.75 mm at the optimal diastolic phase. Centerline and luminal contours for coronary arteries ≥2 mm in diameter were automatically generated. Two observers (F.Z and X.L.Z), blinded to the results of invasive FFR, independently measured the $cFFR_{ML}$ values in each patient according to the location where the invasive FFR measurements were taken. The

mean $cFFR_{ML}$ values from the two observers were used in the final analysis. Moreover, the $cFFR_{ML}$ values of the vessels without invasive FFR measurement were measured at the site distal to the main lesion or distal vessels if no lesion was present.

2.4. Invasive coronary angiography and fractional flow reserve measurements

Invasive coronary angiography and FFR were performed according to standard practice [6]. FFR measurements were performed using 6 or 7 F guiding catheters and intravenous adenosine triphosphate was injected manually through the guiding catheter. The FFR pressure-wire was positioned at a minimum of 20 mm distal to the stenosis in vessel segments ≥2 mm. Hyperaemia was induced by intravenous adenosine triphosphate (140–180 mg/kg/min). FFR ≤ 0.80 was defined as lesion-specific ischemia [5].

2.5. Statistical analysis

Statistical analysis was performed using commercial software (MedCalc; Version 17.6). The Kolmogorov-Smirnov test was conducted to assess the normality of the quantitative data. Quantitative variables were expressed as mean ± SD if normally distributed; while median and inter-quartile range [IQR] was provided for non-normally distributed data. Sensitivity, specificity, positive predictive value (PPV), negative predictive value (NPV) and accuracy at both a per-patient basis and per-vessel basis with invasive FFR as the reference standard were calculated. Inter-observer agreement was also acquired with interclass correlation coefficient (ICC). Pearson's correlation coefficient and Bland-Altman analysis were used to analyze the correlation and agreement between $cFFR_{ML}$ and invasive FFR measurements, respectively. The optimal threshold of CT-FFR to determine functional significance of stenosis was calculated using the Youden index, the area under the curve (AUC) was compared between the optimal threshold of CT-FFR and standard threshold of 0.8 by Delong test. P ≤ 0.05 was considered statistically significant.

3. Meta-analysis

3.1. Search strategy

Following the general PRISMA [25] and MOOSE [26] guidelines for meta-analysis, we searched electronic databases including Web of Science, PubMed, and the Cochrane Library up to 31 March 2018 with no restriction on language. The searching terms included "computed tomography derived fractional flow reserve" or "CT derived fractional flow reserve" or "noninvasive fractional flow reserve" or "noninvasive FFR". The final decision on inclusion was reached through consensus of the two screening authors (L.J.Z and C.X.T). Reviews, case reports, editorial comments, meeting abstracts, letters and authors' replies were excluded. Potential references were hand-searched by two independent reviewers to evaluate if they met the inclusion/exclusion criteria. The flowchart of the study selection was shown in Fig. 1.

3.2. Data extraction and quality assessment

Original data from the included studies were extracted into predefined data extraction forms, which consist of 1) study characteristics, 2) patient characteristics, 3) diagnostic performance measurements on CT-FFR and CCTA with invasive FFR ≤ 0.8 and 4) agreements between invasive FFR and CT-FFR values. Full text reading and data extraction were accomplished by two experienced radiologists (L.J.Z and C.X.T). Risk of bias was independently assessed by L.J.Z and C.X.T using the Quality Assessment of Diagnostic Accuracy Studies, Version 2 (QUADAS-2) [27] comprising four key domains: patient selection, index test, reference standard, and flow and timing. Each domain was assessed for risk of bias, and the first three were evaluated for applicability. Signaling questions were included to inform judgments regarding risk of bias: a domain would be rated "high risk of bias" if the response to a nested signaling question was "No". Any disagreement in quality assessment was resolved via consensus.

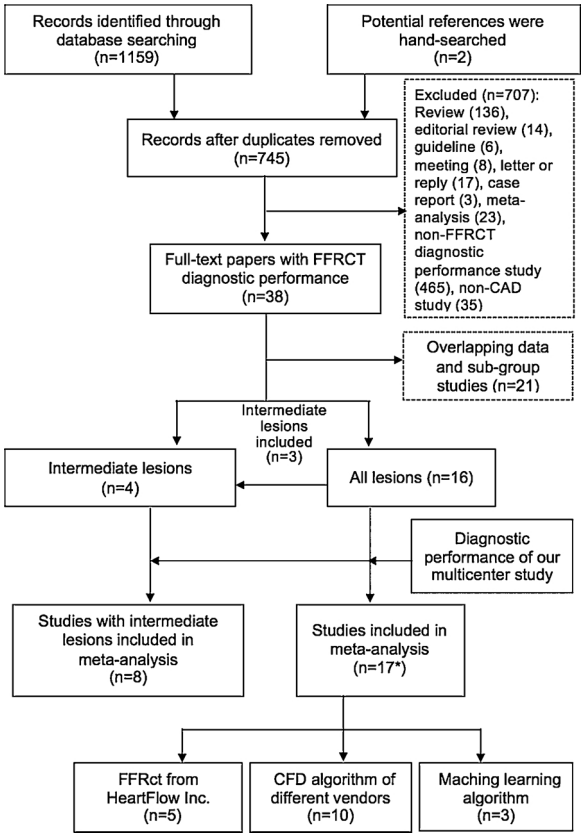

Fig. 1. Flowchart of the article search and selection process utilized for the meta-analysis.
CT-FFR: coronary CT angiography derived fractional flow reserve; CCTA: coronary CT angiography; FFR_{CT}: Fractional flow reserve derived from coronary CT angiography; CFD: computational fluid dynamics.
*indicates that CFD and machine learning algorithms were both applied in one of the studies included in the meta-analysis.

3.3. Statistical analysis

The meta-analysis of diagnostic performance was carried out at a per-patient and a per-vessel level. Diagnostic measurements such as sensitivity, specificity, positive likelihood ratio (LR+), negative likelihood ratio (LR−), diagnostic odds ratio (DOR), accuracy, summary receiver operating characteristic (SROC) curve and their 95% confidence intervals (CI) were extracted directly from the publications or calculated indirectly from the information given. Correlation coefficient and 95% CIs were extracted and calculated. Pooled estimates were determined using a bivariate model. Study heterogeneity was assessed by a bivariate meta-regression model. The heterogeneity of the values between studies was determined by calculating the Q statistic, derived from the χ^2 test, and the inconsistency index (I^2). A P ≤ 0.05 or an $I^2 > 50\%$ suggested heterogeneity, if heterogeneity existed, random effects were used; if not, then fixed effects were reported. In a subgroup analysis, studies were stratified by the following: (a) intermediate lesions, (b) different algorithms of CT-FFR, including FFR_{CT}, CFD from different algorithms and machine learning algorithm. Paired Mcnemar test was used to compare pooled diagnostic performance between CT-FFR and CCTA on a per-vessel basis. χ^2 test was also used to compare the difference among the diverse CT-FFR algorithms generated by the

Table 1
Patient demographics.

Basic characteristics	Numbers
Age, yrs	60.6 ± 8.6
Sex (male), n (%)	100 (73.5%)
Body Mass Index	25.5 ± 3.4
Cardiovascular risk factors, n (%)	
Diabetes	36 (26.5%)
Hypertension	89 (65.4%)
Current-smoker	60 (44.1%)
Hypercholesterolemia	56 (41.2%)
Prior myocardial infarction	4 (2.9%)
Chest pain, n (%)	
Typical angina	69 (50.7%)
Atypical angina	35 (25.7%)
Nonanginal chest pain	5 (3.7%)
Others (Dyspnea)	1 (0.7%)
Asymptomatic	11 (8.1%)
Electrocardiography, n (%)	
ST-T segment change	33 (24.3%)
T wave change	7 (5.1%)
CT angiography	
Nitroglycerin before CTA, n (%)	136 (100%)
Heart rate, bpm	68.2 ± 9.8
Agatston score*, n (%)	
0-399	36 (73.5%)
400-799	7 (14.3%)
> 799	6 (12.2%)
Vessel location, n (%)	
LM/LAD	72 (52.9%)
LCX	11 (8.1%)
RCA	17 (12.5%)
Multi-vessels	36 (26.5%)
Lesion location, n (%)	
Proximal	49 (36.0%)
Middle	53 (39.0%)
Distal	15 (11.0%)
Multi-lesions	19 (14.0%)
cFFR ≤ 0.8	56 (41.2%)
Invasive coronary angiography, n (%)	
Stenosis degree (visually assessed in invasive angiography, %)	
< 50%	12 (8.8%)
≥ 50%	124 (91.2%)
FFR ≤ 0.8	57 (41.9%)

* Indicates that Agatston score was obtained in 49 patients.

individual vendors. A Deeks' funnel plot was used to assess the likelihood of publication bias for both at a per-vessel and a per-patient level. All statistical analyses were performed using STATA version 14 (StataCorp LP, College Station, TX 77845, USA) with the Midas package.

4. Results

4.1. Patient and lesion characteristics

The final patient population consisted of 183 vessels in 136 patients (mean age: 60.6 ± 8.6 years old, 73.5% male) with invasive FFR as reference standard. The severity of coronary lesions evaluated by CCTA and ICA ranged from 20% to 90% luminal narrowing. Invasive FFR interrogation assessed the presence of hemodynamically stenosis (FFR ≤ 0.80) in 67 vessels of 57 patients. The relevant results of CCTA and invasive FFR are displayed in Table 1.

4.2. The diagnostic performance of $cFFR_{ML}$ meansurements and CCTA, and inter-observer agreement

The optimal threshold computed with the Youden index was 0.805 for both per-patient and per-vessel basis, however in this study the standard threshold of 0.80 was used due to no significant difference between the optimal threshold and standard threshold with the same AUC of 0.88 (95% CI: 0.81˜0.93) on a per-patient basis and with the same AUC of 0.89 (95% CI: 0.83˜0.93) on a per-vessel basis (both P > 0.999). Median invasive FFR and $cFFR_{ML}$ values were 0.81 [IQR: 0.74 to 0.86], 0.81 [IQR: 0.74 to 0.87] on a per-patient basis and 0.82 [IQR: 0.76 to 0.87], 0.84 [IQR: 0.76 to 0.89] on a per-vessel basis. According to invasive FFR, the sensitivities, specificities, accuracies, PPVs, NPVs of $cFFR_{ML}$ and CCTA were 0.84, 0.94, 0.90, 0.90, 0.90 and 0.95, 0.28, 0.55, 0.47, 0.88 on a per-vessel basis. The specific diagnostic performance of $cFFR_{ML}$ and CCTA with invasive FFR as the reference standard are reported in Table 2. A representative case was displayed in Fig. 2.

The Pearson correlation coefficient between mean $cFFR_{ML}$ and invasive FFR on a per-vessel basis was 0.84 (95% CI: 0.79˜0.88). Supplementary Fig. 2 also showed results from Bland-Altman analysis on both per-patient and per-vessel basis. Inter-observer agreement were good on a per-patient basis (ICC: 0.94, 95% CI: 0.93˜0.95) and a per-

Table 2
Diagnostic performance of $cFFR_{ML}$ (≤ 0.8) and CCTA (> 50% stenosis) in the detection of hemodynamic relevant coronary artery stenosis in our multicenter study with invasive FFR as reference standard (≤ 0.8).

			Statistical results (95% CI)									
Analysis basis		Modality	TP	TN	FR	FN	Sen.	Spec.	Acc.	PPV	NPV	AUC
All lesions	**Per-patient**	**$cFFR_{ML}$**	**55**	**66**	**6**	**9**	0.86 (0.75˜0.92)	0.92 (0.83˜0.96)	0.89 (0.83˜0.93)	0.90 (0.80˜0.95)	0.88 (0.79˜0.94)	0.95 (0.92˜0.98)
		CCTA	**61**	**24**	**48**	**3**	0.95 (0.87˜0.98)	0.33 (0.24˜0.45)	0.63 (0.54˜0.70)	0.56 (0.47˜0.65)	0.89 (0.72˜0.96)	0.64 (0.55˜0.74)
	Per-vessel	**$cFFR_{ML}$**	**63**	**102**	**7**	**11**	0.84 (0.75˜0.93)	0.94 (0.87˜0.97)	0.90 (0.85˜0.94)	0.90 (0.80˜0.95)	0.90 (0.83˜0.95)	0.95 (0.92˜0.98)
		CCTA	**70**	**30**	**79**	**4**	0.95 (0.87˜0.98)	0.28 (0.20˜0.37)	0.55 (0.47˜0.62)	0.47 (0.39˜0.55)	0.88 (0.73˜0.95)	0.61 (0.53˜0.69)
Intermediate lesions	**Per-patient**	**$cFFR_{ML}$**	**32**	**58**	**5**	**6**	0.84 (0.70˜0.93)	0.92 (0.83˜0.97)	0.89 (0.82˜0.94)	0.87 (0.72˜0.94)	0.91 (0.81˜0.96)	0.95 (0.91˜0.99)
		CCTA	**37**	**22**	**41**	**1**	0.97 (0.87˜1.00)	0.35 (0.24˜0.47)	0.58 (0.49˜0.68)	0.47 (0.37˜0.58)	0.96 (0.79˜0.99)	0.66 (0.56˜0.77)
	Per-vessel	**$cFFR_{ML}$**	**33**	**76**	**5**	**8**	0.81 (0.66˜0.90)	0.94 (0.86˜0.97)	0.89 (0.83˜0.94)	0.87 (0.73˜0.94)	0.91 (0.82˜0.95)	0.96 (0.92˜0.99)
		CCTA	**39**	**25**	**56**	**2**	0.95 (0.84˜0.99)	0.31 (0.22˜0.42)	0.52 (0.44˜0.61)	0.41 (0.32˜0.51)	0.93 (0.77˜0.98)	0.63 (0.53˜0.73)

$cFFR_{ML}$: computational fractional flow reserve based on machine learning; CCTA: coronary CT angiography.
TP: true positive; TN: true negative; FP: false positive; FN: false negative; Sen.: sensitivity; Spec.: specificity; Acc.: accuracy; PPV: positive predictive value; NPV: negative predictive value; AUC: area under the curve.
Values in parenthesis indicate 95% confidence interval.

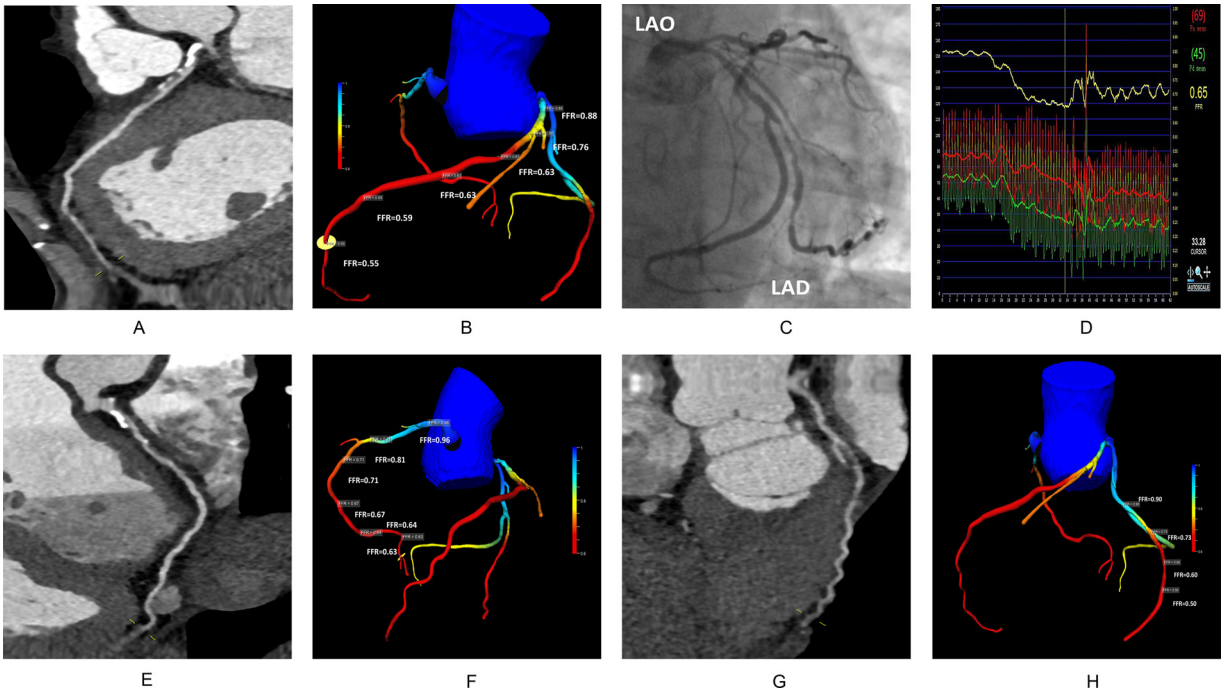

Fig. 2. Representative images used to assess the diagnostic performance of CCTA and $cFFR_{ML}$.
61-year-old male with known CAD who underwent CCTA. Panel a curved multiplanar reformatted image of LAD showing a long mixed plaque (arrows) in the proximal segment causing intermediate stenosis, FFR values of different sites of the LAD measured with $cFFR_{ML}$ are given in panel b; panel c, DSA shows 60% stenosis in the proximal LAD and 80% stenosis in the middle LAD, and invasive FFR value of 0.65, measured in the mid LAD (panel d), similar to $cFFR_{ML}$. Panels e, g indicate that multiple mixed plaques in the proximal RCA and LCX (arrows), correspond to decreased $cFFR_{ML}$ values (panel f, panel h), implying that lesions in multiple vessels in the same patients may lead to myocardial ischemia.
LAO: left anterior oblique.

vessel basis (ICC: 0.94, 95% CI: 0.92˜0.96).

4.3. The diagnostic performance of $cFFR_{ML}$ meansurements on intermediate lesions

Intermediate lesions were identified in 122 vessels in 101 patients on CCTA with stenosis severity between 30%˜70%. The specific diagnostic performances for intermediate lesions on a per-patient basis and on a per-vessel basis using $cFFR_{ML}$ and CCTA with invasive FFR were reported in Table 2.

4.4. Meta-analysis

4.4.1. Characteristics and quality of the included studies

Our search strategy identified 1161 papers, which were screened for review. The flowchart describing the article search and selection process is given in Fig. 1. Finally, 38 papers were selected for full-text reading. Overall, study characteristics are shown in Supplementary Table 1. The remaining papers were combined with data from our multicenter study. Thus, seventeen papers were ultimately included in the present meta-analysis regarding the diagnostic performance of different CT-FFR algorithms [3–7,9–13,28–33] and 4 papers included for intermediate lesions analysis [34–37] for the detection of functional significant stenosis. Furthermore, the risk of bias for the included studies was low (Supplementary Table 2).

4.4.2. Diagnostic performance of CT-FFR and CCTA

A total of 1418 patients and 2312 vessels were analyzed. Diagnostic performances of CT-FFR and CCTA on a per-patient and a per-vessel basis are summarized in Table 3. On a per-vessel basis, pooled sensitivities, specificities, accuracies of CT-FFR and CCTA were 0.85, 0.82, 0.82, and 0.87, 0.57, 0.65 with AUC of 0.86 (95%CI: 0.83˜0.89) and 0.83 (95%CI: 0.79˜0.86) (Fig. 3), respectively, demonstrating a sizable disparity between these two modalities ($P < 0.001$).

Pearson correlation coefficient between CT-FFR and invasive FFR showed a combined Pearson correlation coefficient of 0.73 (95%CI: 0.67˜0.78) with random effect (Supplementary Fig. 2).

4.4.3. Diagnostic performance of CT-FFR in intermediate lesions and different algorithms

The pooled sensitivities, specificities, accuracies of CT-FFR on a per-vessel basis for intermediate lesions were 0.85, 0.74, 0.82, respectively. In addition, the AUCs are shown in Fig. 3.

On a per-vessel basis, FFR_{CT}, CFD and machine learning algorithms had pooled sensitivities of 0.84, 0.86, 0.85, specificities of 0.73, 0.80, 0.91, and accuracies of 0.79, 0.80, 0.89, respectively (Fig. 3). There was no significant difference between the different algorithms for the pooled sensitivities ($P = 0.843$), while a higher specificity and accuracy of FFR_{CT} derived from machine learning algorithm were found when compared to the CFD algorithm (both $P < 0.001$). No differences were found in specificity ($P = 0.566$) and accuracy ($P = 0.225$) between FFR_{CT} and CFD algorithm.

4.4.4. Assessment of heterogeneity and publication bias

No heterogeneity in pooled sensitivity ($I^2 = 0$, 20.5) and LR- ($I^2 = 4.8$, 42.7) was found both on a per-patient and per-vessel basis of CT-FFR, as well as pooled sensitivity ($I^2 = 0$) LR+ ($I^2 = 38.0$), LR- ($I^2 = 0$) on a per-patient basis. The pooled sensitivity on a per-vessel basis in intermediate lesions also showed a lack of heterogeneity ($I^2 = 0$). Deeks' funnel plots showed no evidence of publication bias at a per-vessel and a per-patient basis (Supplementary Fig. 4).

5. Discussion

In this multi-center study, we investigated a prototype for the computation of FFR derived from CCTA based on a deep machine

Table 3
Pooled diagnostic performance of CT-FFR and CCTA with invasive FFR as reference standard.

			Statistical results (95% CI)					
	Modality	Unit of analysis	Sen.	Spec.	LR+	LR-	DOR	Acc.
All lesions	**CT-FFR**	**Per-patient**	0.90 (0.86˜0.92)	0.78 (0.68˜0.86)	4.2 (2.8˜6.2)	0.13 (0.10˜0.18)	31 (18˜55)	0.82 (0.79˜0.84)
		Per-vessel	0.85 (0.83˜0.88)	0.82 (0.76˜0.87)	4.5 (3.2˜6.3)	0.18 (0.16˜0.22)	25 (16˜40)	0.81 (0.79˜0.83)
	CCTA	**Per-patient**	0.90 (0.80˜0.95)	0.32 (0.19˜0.50)	1.4 (1.3˜1.6)	0.29 (0.19˜0.45)	5 (3˜8)	0.62 (0.58˜0.66)
		Per-vessel	0.87 (0.77˜0.93)	0.57 (0.38˜0.74)	2.0 (1.4˜2.7)	0.27 (0.20˜0.37)	7 (4˜12)	0.65 (0.62˜0.68)
Intermediate lesions	**CT-FFR**	**Per-patient**	0.85 (0.79˜0.90)	0.81 (0.72˜0.87)	4.5 (3.0˜6.7)	0.19 (0.13˜0.27)	24 (23˜47)	0.82 (0.78˜0.85)
		Per-vessel	0.87 (0.82˜0.91)	0.81 (0.70˜0.89)	4.3 (3.1˜5.9)	0.18 (0.14˜0.23)	24 (14˜39)	0.80 (0.73˜0.85)
Different algorithms	**FFR_{CT}**	**Per-patient**	0.89 (0.85˜0.93)	0.70 (0.65˜0.75)	3.0 (2.5˜3.6)	0.15 (0.11˜0.22)	20 (13˜31)	0.79 (0.74˜0.83)
	CFD		0.93 (0.86˜0.96)	0.78 (0.69˜0.85)	4.2 (2.9˜6.0)	0.09 (0.05˜0.18)	46 (19˜107)	0.85 (0.80˜0.90)
	ML		–	–	–	–	–	–
	FFR_{CT}	**Per-vessel**	0.84 (0.80˜0.88)	0.73 (0.60˜0.84)	3.2 (2.0˜5.0)	0.22 (0.16˜0.30)	15 (7˜30)	0.79 (0.76˜0.81)
	CFD		0.86 (0.82˜0.89)	0.82 (0.72˜0.86)	4.3 (3.1˜5.9)	0.18 (0.14˜0.23)	24 (14˜39)	0.80 (0.73˜0.85)
	ML		0.85 (0.78˜0.90)	0.91 (0.87˜0.94)	9.4 (6.4˜13.9)	0.17 (0.11˜0.25)	57 (30˜107)	(0.85˜0.92)

- indicates that diagnostic performance of CT-FFR on a per-patient basis was obtained from the first two algorithms since not enough records about machine learning could be included in the meta-analysis.
CT-FFR: coronary CT angiography derived fractional flow reserve ; CCTA: coronary CT angiography.
FFR_{CT}: fractional flow reserve derived from coronary CT angiography; CFD: computational fluid dynamics; ML: machine learning.
CI: confidence interval; Sen.: sensitivity; Spec.: specificity; Acc.: accuracy; PPV: positive predictive value; NPV: negative predictive value.
LR+: positive likelihood ratio; LR-: negative likelihood ratio; DOR: diagnostic odds ratio.

learning method with invasive FFR as the reference standard. In addition, we compared the combined diagnostic performance of different CT-FFR algorithms and CCTA to estimate lesion-specific ischemia with a meta-analysis by combining the results obtained from multiple studies. Our study demonstrated that 1) $cFFR_{ML}$ had a high diagnostic accuracy in determining lesion-specific ischemia in CAD compared with CCTA alone and in intermediate lesions; 2) no significant difference was found for combined diagnostic performance among different CT-FFR algorithms. To date, this is the first study to estimate ischemia-specific lesion with $cFFR_{ML}$ integrated into a meta-analysis and comprehensively to compare combined diagnostic performance of the main CT-FFR algorithms, including FFR_{CT}, CFD algorithm from different vendors and machine learning algorithm (Fig. 4).

The general diagnostic performance of machine learning algorithm of CT-FFR noninvasive artificial-intelligence algorithm has been previously investigated with sensitivity and specificity ranging from 0.79˜0.91 and 0.76˜0.96 on a per-vessel basis, respectively [12–14,38]. Our multicenter study also validated the performance of noninvasive machine learning based CT-FFR with excellent sensitivity and specificity of 0.84 and 0.94, suggesting this technique as a promising tool with instant availability and clinical utility to determine lesion-specific ischemia.

Prior meta-analysis showed the range of pooled sensitivity and specificity with CT-FFR in detecting lesion-specific ischemia were 0.89˜0.9 and 0.7˜0.73 on a per-patient basis, and 0.82˜0.84 and 0.76˜0.79 on a per-vessel basis [17,19–21]. Moreover, the range of pooled sensitivity and specificity with CCTA were reported with 0.89˜0.92 and 0.35˜0.61 on a per-patient basis, and 0.87˜0.91 and 0.56˜0.65 on a per-vessel basis [17,19–21]. Our meta-analysis showed similar sensitivity (0.9 vs. 0.9), slightly higher specificity on per-patient basis (0.78 vs. 0.73,) and slightly higher sensitivity (0.85 vs. 0.84) and specificity (0.82 vs. 0.79) on a per vessel basis of CT-FFR when compared to the prior meta-analysis results. Furthermore, our study included a larger sample size, incorporated more recent clinical studies and utilized more CT-FFR algorithms.

Since the clinical implementation of invasive FFR-guided revascularization is only 10%–20% [2], noninvasive CT-FFR algorithms from various vendors may increase the quality of patient care and decrease costs and change patient logistics. Recently different vendors have begun generating multiple CT-FFR algorithms; however, only a few studies compared two of the different algorithms [12,12,16,38]. According to Tan et al. [16], the pooled sensitivity (0.73 vs. 0.72, P = 0.04) and pooled specificity (0.93 vs. 0.87, p = 0.01) of FFR_{CT} were higher than CFD algorithm (cFFR, Siemens 1.4). Tesche et al. [14] and Coenen et al. [38] found that the diagnostic performance of machine learning and FFR_{CT} showed no significant difference on a per-lesion and per-patient level, and both outperformed standard conventional CCTA evaluation. Itu et al. [12] also compared diagnostic performance between CFD and deep machine learning algorithms of cFFR (Siemens), and no difference between these two algorithms. In general, our meta-analysis results showed similar pooled sensitivity of FFR_{CT}, CFD algorithms from different vendors and machine learning algorithm. In addition, the results demonstrated higher specificity and accuracy of the machine learning approach compared with FFR_{CT} and CFD algorithm from different vendors. Moreover, our meta-analysis results also showed no difference between FFR_{CT} and CFD algorithm

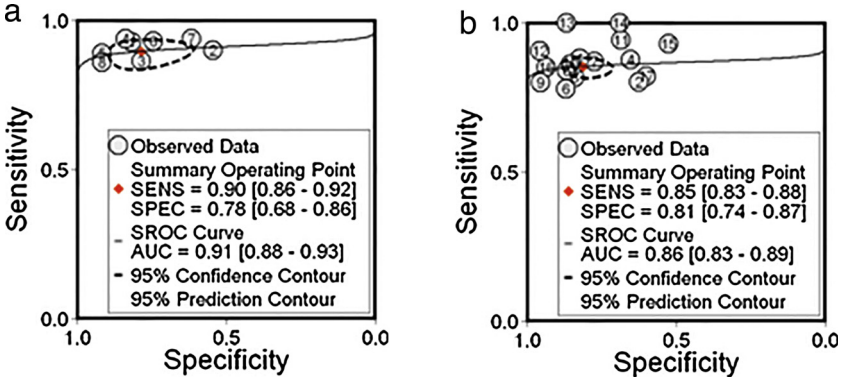

Fig. 3. SROC curve on per-patient and per-vessel basis of CT-FFR.
Panel a, SROC curve shows combined sensitivity and specificity of CT-FFR were 0.90 and 0.78, on a per-patient basis; while panel b shows combined sensitivity of 0.85 and specificity of 0.81 on a per-vessel basis.
SROC curve: summary receiver operating characteristic curve; CI: confidence interval.

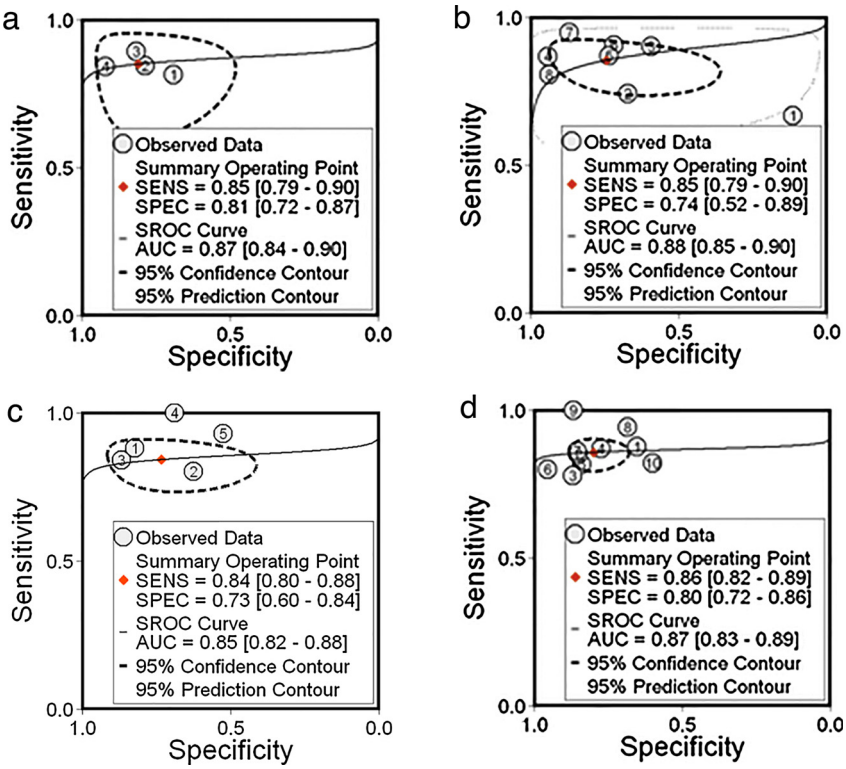

Fig. 4. SROC curve of CT-FFR in intermediate lesions on a per-patient and per-vessel basis and of different CT-FFR algorithms on a per-vessel basis.
Panel a and b show combined sensitivities and specificities of 0.85, 0.85 and 0.81 0.74, with AUCs of 0.87 and 0.88 on a per-patient and a per-vessel basis in intermediate lesions, respectively. Panel c displays combined sensitivity of 0.84, specificity of 0.73 and AUC of 0.85 with FFR_{CT} on a per-vessel basis. Panel d shows sensitivity, specificity and AUC of 0.86, 0.80, and 0.89 with CFD from different vendors. SROC could not be obtained for the machine learning algorithm due to the limited number of publications about this algorithm.

from different vendors. The difference between our results and the previous study reported by Tan et al. [16] may be due to the inclusion of more CFD algorithms that were derived from other vendors.

There were several limitations to the study that should be considered when interpreting the results. Firstly, the retrospective nature and relatively small sample size of the original multicenter study needs to be mentioned. Secondly, the results from both readers in the multicenter study might be biased for CT-FFR analysis because the position of invasive FFR measurements was not blinded to the readers. Thirdly, selection bias can be present for included patients with 60 years old on average age, cardiovascular risk factors and CAD history. Fourthly, the influence of image quality of CCTA on diagnostic performance was not analyzed due to only good or excellent image quality of CCTA were included. Lastly, not the same amount of papers were included when analyzing the pooled diagnostic performance of different CT-FFR algorithms. In addition, the definition of stenosis severity for intermediate lesions differed across the included studies, ranging from 25% to 70% in size.

In conclusion, although the limitations may affect the results, the machine learning algorithm of CT-FFR had a high diagnostic accuracy in determining ischemia-specific lesion when compared to CCTA alone and performed well in intermediate lesions. Furthermore, there was no significant difference in the diagnostic performance among the different CT-FFR algorithms.

Conflict of interest

U. Joseph Schoepf is a consultant for and / or receives research support from Astellas, Bayer, GE, Guerbet, HeartFlow Inc., and Siemens. The other authors have no conflicts of interest to declare.

Funding

Supported by The National Key Research and Development Program of China (2017YFC0113400 for L.J.Z.; 2016YFC1300300 for L.X).

Appendix A. Supplementary data

Supplementary material related to this article can be found, in the online version, at doi:https://doi.org/10.1016/j.ejrad.2019.04.011.

References

[1] C. Tesche, C.N. De Cecco, M.H. Albrecht, T.M. Duguay, R.R. Bayer 2nd, S.E. Litwin, D.H. Steinberg, U.J. Schoepf, Coronary CT angiography-derived fractional flow reserve, Radiology 285 (1) (2017) 17–33.
[2] N.V. Pothineni, N.N. Shah, Y. Rochlani, R. Nairooz, S. Raina, M.A. Leesar, B.F. Uretsky, A. Hakeem, U.S. trends in inpatient utilization of fractional flow reserve and percutaneous coronary intervention, J. Am. Coll. Cardiol. 67 (6) (2016) 732–733.
[3] B.K. Koo, A. Erglis, J.H. Doh, D.V. Daniels, S. Jegere, H.S. Kim, A. Dunning, T. DeFrance, A. Lansky, J. Leipsic, J.K. Min, Diagnosis of ischemia-causing coronary stenoses by noninvasive fractional flow reserve computed from coronary computed tomographic angiograms. Results from the prospective multicenter DISCOVER-FLOW (Diagnosis of Ischemia-Causing Stenoses Obtained Via Noninvasive Fractional Flow Reserve) study, J. Am. Coll. Cardiol. 58 (19) (2011) 1989–1997.
[4] J.K. Min, J. Leipsic, M.J. Pencina, D.S. Berman, B.K. Koo, C. van Mieghem, A. Erglis, F.Y. Lin, A.M. Dunning, P. Apruzzese, M.J. Budoff, J.H. Cole, F.A. Jaffer, M.B. Leon, J. Malpeso, G.B. Mancini, S.J. Park, R.S. Schwartz, L.J. Shaw, L. Mauri, Diagnostic accuracy of fractional flow reserve from anatomic CT angiography, JAMA 308 (12) (2012) 1237–1245.
[5] B.L. Nørgaard, J. Leipsic, S. Gaur, S. Seneviratne, B.S. Ko, H. Ito, J.M. Jensen, L. Mauri, B. De Bruyne, H. Bezerra, K. Osawa, Diagnostic performance of noninvasive fractional flow reserve derived from coronary computed tomography angiography in suspected coronary artery disease: the NXT trial (Analysis of Coronary Blood Flow Using CT Angiography: Next Steps), J. Am. Coll. Cardiol. 63 (12) (2014) 1145–1155.
[6] A. Coenen, M.M. Lubbers, A. Kurata, A. Kono, A. Dedic, R.G. Chelu, M.L. Dijkshoorn, F.J. Gijsen, M. Ouhlous, R.J. van Geuns, K. Nieman, Fractional flow reserve computed from noninvasive CT angiography data: diagnostic performance of an on-site clinician-operated computational fluid dynamics algorithm, Radiology 274 (3) (2015) 674–683.
[7] M. Renker, U.J. Schoepf, R. Wang, F.G. Meinel, J.D. Rier, R.R. Bayer 2nd, H. Möllmann, C.W. Hamm, D.H. Steinberg, S. Baumann, Comparison of diagnostic value of a novel noninvasive coronary computed tomography angiography method versus standard coronary angiography for assessing fractional flow reserve, Am. J. Cardiol. 114 (9) (2014) 1303–1308.
[8] A. Coenen, M.M. Lubbers, A. Kurata, F.G. Meinel, J.D. Rier, R.R. Bayer 2nd, H. Möllmann, C.W. Hamm, D.H. Steinberg, S. Baumann, Coronary CT angiography derived fractional flow reserve: methodology and evaluation of a point of care algorithm, J. Cardiovasc. Comput. Tomogr. 10 (2) (2016) 105–113.

[9] D.H. Yang, Y.H. Kim, J.H. Roh, J.W. Kang, J.M. Ahn, J. Kweon, J.B. Lee, S.H. Choi, E.S. Shin, D.W. Park, S.J. Kang, S.W. Lee, C.W. Lee, S.W. Park, Diagnostic performance of on-site CT-derived fractional flow reserve versus CT perfusion, Eur. Heart J. Cardiovasc. Imaging 18 (4) (2017) 432–440.
[10] B.S. Ko, J.D. Cameron, R.K. Munnur, D.T.L. Wong, Y. Fujisawa, T. Sakaguchi, K. Hirohata, J. Hislop-Jambrich, S. Fujimoto, K. Takamura, M. Crossett, M. Leung, A. Kuganesan, Y. Malaiapan, A. Nasis, J. Troupis, I.T. Meredith, S.K. Seneviratne, Noninvasive CT-derived FFR based on structural and fluid analysis: a comparison with invasive FFR for detection of functionally significant stenosis, J. Am. Coll. Cardiol. Img. 10 (6) (2017) 663–673.
[11] J.M. Zhang, L. Zhong, T. Luo, A.M. Lomarda, Y. Huo, J. Yap, S.T. Lim, R.S. Tan, A.S. Wong, J.W. Tan, K.K. Yeo, J.M. Fam, F.Y. Keng, M. Wan, Simplified models of non-invasive fractional flow reserve based on CT images, PLoS One 11 (5) (2016) e0153070.
[12] L. Itu, S. Rapaka, T. Passerini, B. Georgescu, C. Schwemmer, M. Schoebinger, T. Flohr, P. Sharma, D. Comaniciu, A machine-learning approach for computation of fractional flow reserve from coronary computed tomography, J. Appl. Physiol. 121 (1) (1985) 42–52 2016.
[13] J. Röther, M. Moshage, D. Dey, C. Schwemmer, M. Tröbs, F. Blachutzik, S. Achenbach, C. Schlundt, M. Marwan, Comparison of invasively measured FFR with FFR derived from coronary CT angiography for detection of lesion-specific ischemia: results from a PC-based prototype algorithm, J. Cardiovasc. Comput. Tomogr. 12 (2) (2018) 101–107.
[14] C. Tesche, C.N. De Cecco, S. Baumann, M. Renker, T.W. McLaurin, T.M. Duguay, R.R. Bayer 2nd, D.H. Steinberg, K.L. Grant, C. Canstein, C. Schwemmer, M. Schoebinger, L.M. Itu, S. Rapaka, P. Sharma, U.J. Schoepf, Coronary CT angiography-derived fractional flow reserve: machine learning algorithm versus computational fluid dynamics modeling, Radiology 288 (1) (2018) 64–72.
[15] M. Kruk, Ł Wardziak, M. Demkow, W. Pleban, J. Pręgowski, Z. Dzielińska, M. Witulski, A. Witkowski, W. Rużyłło, C. Kępka, Workstation-based calculation of CTA-based FFR for intermediate stenosis, J. Am. Coll. Cardiol. Img. 9 (6) (2016) 690–699.
[16] X.W. Tan, Q. Zheng, L. Shi, F. Gao, J.C. Allen, A. Coenen, S. Baumann, U.J. Schoepf, G.S. Kassab, S.T. Lim, A.S.L. Wong, J.W.C. Tan, K.K. Yeo, Combined diagnostic performance of coronary computed tomography angiography and computed tomography derived fractional flow reserve for the evaluation of myocardial ischemia: a meta-analysis, Int. J. Cardiol. 236 (2017) 100–106.
[17] S. Deng, X.D. Jing, J. Wang, C. Huang, S. Xia, J.L. Du, Y.J. Liu, Q. She, Diagnostic performance of noninvasive fractional flow reserve derived from coronary computed tomography angiography in coronary artery disease: a systematic review and meta-analysis, Int. J. Cardiol. 184 (2015) 703–709.
[18] J.A. Gonzalez, M.J. Lipinski, L. Flors, P.W. Shaw, C.M. Kramer, M. Salerno, Meta-analysis of diagnostic performance of coronary computed tomography angiography, computed tomography perfusion, and computed tomography-fractional flow reserve in functional myocardial ischemia assessment versus invasive fractional flow reserve, Am. J. Cardiol. 116 (2015) 1469–1478.
[19] H.B. Panchal, S.P. Veeranki, S. Bhatheja, N. Barry, E. Mahmud, M. Budoff, S.J. Lavine, H.M. Mamudu, T.K. Paul, Fractional flow reserve using computed tomography for assessing coronary artery disease: a meta-analysis, J. Cardiovasc. Med. (Hagerstown) 17 (9) (2016) 694–700.
[20] A. Ding, G. Qiu, W. Lin, L. Hu, G. Lu, X. Long, X. Hong, Y. Chen, X. Luo, Q. Tang, D. Deng, Diagnostic performance of noninvasive fractional flow reserve derived from coronary computed tomography angiography in ischemia-causing coronary stenosis: a meta-analysis, J. Radiol. 34 (12) (2016) 795–808.
[21] I. Danad, J. Szymonifka, J.W.R. Twisk, B.L. Norgaard, C.K. Zarins, P. Knaapen, J.K. Min, Diagnostic performance of cardiac imaging methods to diagnose ischaemia-causing coronary artery disease when directly compared with fractional flow reserve as a reference standard: a meta-analysis, Eur. Heart J. 38 (13) (2017) 991–998.
[22] J. Lee, K.W. Kim, S.H. Choi, J. Huh, S.H. Park, Systematic review and meta-analysis of studies evaluating diagnostic test accuracy: a practical review for clinical researchers–part II. Statistical methods of meta-analysis, Korean J. Radiol. 16 (6) (2015) 1188–1196.
[23] L.J. Zhang, Y. Wang, U.J. Schoepf, F.G. Meinel, R.R. Bayer 2nd, L. Qi, J. Cao, C.S. Zhou, Y.E. Zhao, X. Li, J.B. Gong, Z. Jin, G.M. Lu, Image quality, radiation dose, and diagnostic accuracy of prospectively ECG-triggered high-pitch coronary CT angiography at 70 kVp in a clinical setting: comparison with invasive coronary angiography, Eur. Radiol. 26 (3) (2016) 797–806.
[24] S.M. Benton Jr, C. Tesche, C.N. De Cecco, T.M. Duguay, U.J. Schoepf, R.R. Bayer 2nd, Noninvasive derivation of fractional flow reserve from coronary computed tomographic angiography: a review, J. Thorac. Imaging 33 (2) (2018) 88–96.
[25] D. Moher, A. Liberati, J. Tetzlaff, D.G. Altman, PRISMA Group, Preferred reporting items for systematic reviews and meta-analyses: the PRISMA statement, Ann. Intern. Me. 151 (4) (2009) 264–269.
[26] D.F. Stroup, J.A. Berlin, S.C. Morton, I. Olkin, G.D. Williamson, D. Rennie, D. Moher, B.J. Becker, T.A. Sipe, S.B. Thacker, Meta analysis of observational studies in epidemiology: a proposal for reporting. Meta analysis of observational studies in epidemiology (MOOSE) group, JAMA 283 (15) (2000) 2008–2012.
[27] P.F. Whiting, A.W. Rutjes, M.E. Westwood, S. Mallett, J.J. Deeks, J.B. Reitsma, M.M. Leeflang, J.A. Sterne, P.M. Bossuyt, QUADAS-2 Group, QUADAS-2: a revised tool for the quality assessment of diagnostic accuracy studies, Ann. Intern. Med. 155 (8) (2011) 529–536.
[28] J.H. Chung, K.E. Lee, C.W. Nam, J.H. Doh, H.I. Kim, S.S. Kwon, E.B. Shim, E.S. Shin, Diagnostic performance of a novel method for fractional flow reserve computed from noninvasive computed tomography angiography (NOVEL-FLOW study), Am. J. Cardiol. 120 (2017) 362–368.
[29] C. Shi, D. Zhang, K. Cao, T. Zhang, L. Luo, X. Liu, H. Zhang, A study of noninvasive fractional flow reserve derived from a simplified method based on coronary computed tomography angiography in suspected coronary artery disease, Biomed. Eng. Online 16 (1) (2017) 43.
[30] A. Kurata, A. Coenen, M.M. Lubbers, K. Nieman, T. Kido, T. Kido, N. Yamashita, K. Watanabe, G.P. Krestin, T. Mochizuki, The effect of blood pressure on non-invasive fractional flow reserve derived from coronary computed tomography angiography, Eur. Radiol. 27 (4) (2017) 1416–1423.
[31] K. Osawa, T. Miyoshi, T. Miki, Y. Koide, Y. Kawai, K. Ejiri, M. Yoshida, S. Sato, S. Kanazawa, H. Ito, Coronary lesion characteristics with mismatch between fractional flow reserve derived from CT and invasive catheterization in clinical practice, Heart Vessels 32 (4) (2017) 390–398.
[32] T. Kawaji, H. Shiomi, H. Morishita, T. Morimoto, C.A. Taylor, S. Kanao, K. Koizumi, S. Kozawa, K. Morihiro, H. Watanabe, J. Tazaki, M. Imai, N. Saito, S. Shizuta, K. Ono, K. Togashi, T. Kimura, Feasibility and diagnostic performance of fractional flow reserve measurement derived from coronary computed tomography angiography in real clinical practice, Int. J. Cardiovasc. Imaging 33 (2) (2017) 271–281.
[33] A. Coenen, A. Rossi, M.M. Lubbers, A. Kurata, A.K. Kono, R.G. Chelu, S. Segreto, M.L. Dijkshoorn, A. Wragg, R.M. van Geuns, F. Pugliese, K. Nieman, Integrating CT myocardial perfusion and CT-FFR in the work-up of coronary artery disease, J. Am. Coll. Cardiol. Img. 10 (7) (2017) 760–770.
[34] G. Xia, D. Fan, X. Yao, G. Guan, J. Wang, Diagnostic efficacy of fractional flow reserve with coronary angiography in dual-source computed tomography scanner, Acta Cardiol. 73 (1) (2018) 76–83.
[35] P.M. Donnelly, M. Kolossváry, J. Karády, P.A. Ball, S. Kelly, D. Fitzsimons, M.S. Spence, C. Celeng, T. Horváth, B. Szilveszter, Experience with an on-site coronary computed tomography-derived fractional flow reserve algorithm for the assessment of intermediate coronary stenosis, Am. J. Cardiol. 121 (1) (2018) 9–13.
[36] S. Kishi, A.A. Giannopoulos, A. Tang, N. Kato, Y.S. Chatzizisis, C. Dennie, Y. Horiuchi, K. Tanabe, J.A.C. Lima, F.J. Rybicki, D. Mitsouras, Fractional flow reserve estimated at coronary CT angiography in intermediate lesions: comparison of diagnostic accuracy of different methods to determine coronary flow distribution, Radiology 287 (1) (2018) 76–84.
[37] R. Nakazato, H.B. Park, D.S. Berman, H. Gransar, B.K. Koo, A. Erglis, F.Y. Lin, A.M. Dunning, M.J. Budoff, J. Malpeso, J. Leipsic, J.K. Min, Noninvasive fractional flow reserve derived from computed tomography angiography for coronary lesions of intermediate stenosis severity: results from the DeFACTO study, Circ. Cardiovasc. Imaging 6 (6) (2013) 881–889.
[38] A. Coenen, Y.H. Kim, M. Kruk, C. Tesche, J. De Geer, A. Kurata, M.L. Lubbers, J. Daemen, L. Itu, S. Rapaka, P. Sharma, C. Schwemmer, A. Persson, U.J. Schoepf, C. Kepka, D. Hyun Yang, K. Nieman, Diagnostic accuracy of a machine-learning approach to coronary computed tomographic angiography-based fractional flow reserve: result from the MACHINE consortium, Circ. Cardiovasc. Imaging 11 (6) (2018) e007217.